A Bioinspired Strategy for Directional Charge Propagation in Photoelectrochemical Devices Using Supramolecular Machinery

Tessel Bouwens
University of Amsterdam
Tijmen Bakker
University of Amsterdam https://orcid.org/0000-0001-9294-4073
Jenny Hasenack
University of Amsterdam
Mees Dieperink
University of Amsterdam
Simon Mathew
University of Amsterdam
Joost Reek (j.n.h.reek@uva.nl)
University of Amsterdam https://orcid.org/0000-0001-5024-508X

Article

Keywords: Molecular photoelectrochemical (PEC) devices, photoinduced electron transfer (PET), causing losses in power conversion efficiency (PCE)

Posted Date: February 19th, 2021

DOI: https://doi.org/10.21203/rs.3.rs-228311/v1

Version of Record: A version of this preprint was published at Nature Chemistry on October 27th, 2022.
See the published version at https://doi.org/10.1038/s41557-022-01068-y.

Abstract

Molecular photoelectrochemical (PEC) devices are hampered by electron–hole recombination after photoinduced electron transfer (PET), causing losses in power conversion efficiency (PCE). Inspired by natural photosynthesis, we demonstrate the use of molecular machinery as a strategy to inhibit recombination, through organization of molecular components and unbinding of the final electron acceptor after reduction. We show that preorganization of the macrocyclic **3-NDI-ring** electron acceptor to the $\mathbf{P_{STATION}}$ dye forming the $\mathbf{P_{STATION}}$:**3-NDI-ring** pseudorotaxane, enables a "ring launching" event, upon PET from $\mathbf{P_{STATION}}$ to **3-NDI-ring** releasing **3-NDI-ring**$^{\bullet-}$. Implementing $\mathbf{P_{STATION}}$:**3-NDI-ring** into *p*-type dye-sensitized solar cells (*p*-DSSCs) revealed a fivefold increase in PCE compared to benchmark dye **P1**, unable to facilitate pseudorotaxane formation. This active repulsion of anionic **3-NDI-ring**$^{\bullet-}$ with concomitant reformation $\mathbf{P_{STATION}}$:**3-NDI-ring** circumvents recombination at semiconductor–dye interface, affording a twofold enhancement in hole lifetime. We envision this concept of supramolecular-directed charge-propagation will encourage further integration of molecular machinery into PEC devices.

Introduction

Artificial photosynthesis aims to create photoelectrochemical (PEC) devices for the conversion of solar energy into fuels, using the natural photosynthetic process as a blueprint.[1] One of the challenges in PEC devices is efficient charge separation with concomitant suppression of competing charge recombination,[2] required for the generation of both photocurrent and redox potential to drive energetically uphill, fuel-forming reactions. The natural photosynthetic apparatus promotes effective charge separation through the organization of pigments and electron acceptors in specific geometries via supramolecular interactions (Fig. 1a). Photosystem II (PSII) uses the plastoquinone/hydroquinone (Q_B/QH_2, Fig. 1a) redox couple to spatially remove electrons after photoinduced charge separation at the reaction center. The terminal electron accepting Q_B is hydrogen bound within the PSII protein, close to the plastoquinone A (Q_A, Fig. 1a).[3,4] After two consecutive proton coupled electron transfer events, Q_B is reduced to hydroquinone QH_2, and the affinity for the binding pocket of PSII is lost.[5] The liberated QH_2 diffuses away to participate in subsequent redox chemistry (at Cytochrome b_6f, Fig. 1a), and the PSII binding pocket is occupied by another Q_B for the subsequent photocycle. Mimicking this photoinduced supramolecular control of docking-and-release events of a redox mediator may represent a viable strategy for reducing charge recombination improving power conversion efficiencies (PCEs) in PEC devices.

Dye-sensitized solar cells (DSSCs) are PEC devices with operational principles that parallel natural photosynthesis; a) light absorption is achieved by molecular components (Fig. 1c), b) photocurrent generation is initiated by a photoinduced electron transfer and c) electron transport is accomplished by means of a molecular redox couple, e.g. I^-/I_3^- instead of the Q_B/QH_2 employed by PSII. While the TiO_2-based *n*-type DSSCs (*n*-DSSC) exhibit PCE up to 14.3%,[6] those of the complementary, NiO-based *p*-type

DSSC (*p*-DSSC) are typically 1–2 orders of magnitude lower. This disparity precludes efficiency improvements in tandem DSSCs and artificial photosynthetic PEC devices. The origins of PCE differences between *n*- and *p*-DSSCs is attributed to the charge carrier characteristics of the semiconductor, with very slow (4×10^{-8} cm^2 s^{-1})[7] charge (hole) diffusion in NiO compared to that in TiO_2 (electron diffusion 10^{-4} cm^2 s^{-1}).[8] As a result of this slow hole transport, charge recombination at the semiconductor–electrolyte interface is a much larger issue in NiO-based *p*-DSSC (Fig. 1c, Pathway 5 & 6).[9,10] The natural photosystem circumvents undesirable recombination pathways by preorganizing the redox mediator Q_B at the electron-accepting docking site, followed by unbinding of the reduction product QH_2, effectively separating the charges spatially. In contrast, the DSSC relies on collisional electron transfer under diffusional control, making the restrictive process mass transfer of the reduced redox mediator species away from the semiconductor surface to the counter electrode for regeneration. Former studies imply that dye–mediator interactions between dye and redox mediator could have a favorable effect for the overall PCE of both *n*- and *p*-DSSC.[11–14]

The stimulated binding and unbinding events found in the natural photosystem are of central importance in the field of artificial molecular machines. These include extraordinary examples of functional architectures including molecular pumps[15,16], propellors,[17,18] robotic arms[19], molecular muscles [20,21]and a nanocar.[22] Essential for the function of these molecular machines is the reversible bond, whose dynamic nature allows for molecular motion upon a chemical, electrochemical or photochemical stimulus.[23,24] An example relevant to the work at hand is the photoelectrochemical trigger that leads to the reduced affinity of a macrocycle for a binding site in (pseudo)rotaxane structures, resulting in molecular ring launching or shuttling events.[25,26]

The question that we address in this paper is if pseudorotaxane motifs can be used as molecular machinery, engendering the preorganization and launching of redox mediators in a *p*-DSSC, effectively emulating the docking and active replacement of the electron carrying Q_B/QH_2 redox couple in PSII. For this we utilize macrocyclic redox mediator (**3-NDI-ring)** that threads onto the dye $\mathbf{P_{STATION}}$ to form the $\mathbf{P_{STATION}}$**:3-NDI-ring** pseudorotaxane (Fig. 1b). Directional electron transport in the PEC device is established by the inbuilt free-energy impetus that actively shuttles reduced redox mediator **3-NDI-ring**$^{\bullet-}$ away from the thread, promoting movement away from the semiconductor–dye interface. Finally, the thread favorably binds the next neutral **3-NDI-ring** molecule to reform the pseudorotaxane. Application of this concept in a *p*-DSSC results in PCE increases by a factor 5, attributable to reduced interfacial charge recombination phenomena (Fig. 1b–c).

Results And Discussion

Design and synthesis. The *p*-DSSCs in this study are based on the well documented **P1** dye (Fig. 1e), and as such, the design of the molecular machinery started with this molecular scaffold. The dye $\mathbf{P_{STATION}}$ is an analogue of **P1** where the terminal (dicyano)vinyl electron acceptors are replaced with cyanoacrylate esters to facilitate introduction of a glycol-tethered 1,5-dioxynaphthalene (**DNP**). The **DNP** unit acts as

binding station for electron-deficient molecular rings through the formation of pseudorotaxane suprastructures. The naphthalene diimide-based macrocycle **3-NDI-ring** (Fig. 1e) binds to the **DNP** recognition sites of $\mathbf{P_{STATION}}$, and was designed in an analogous fashion to NDI-based macrocycles previously reported to form pseudorotaxanes with **DNP** recognition sites at the surface–liquid interface.[27,28] As the **3-NDI-ring** functions as redox mediator in the envisioned *p*-DSSC, its redox properties are of key importance, and these compare favorable to those of the typically used I^-/I_3^- (*vide infra*). Thus the proposed **3-NDI-ring**:$\mathbf{P_{STATION}}$ pseudorotaxane photosensitizer (Fig. 1e) is anticipated to improve the PCE of the DSSC device in two ways.[14] Firstly, the **3-NDI-ring** as redox mediator is preorganized close to the dye by the **DNP** recognition sites of $\mathbf{P_{STATION}}$ at the surface–electrolyte interface, favoring charge propagation (Fig. 1b, Step 3) over recombination (Fig. 1c, Pathway 6). Secondly, upon photoexcitation (Fig. 1b, Step 1) and subsequent hole injection into NiO (Fig. 1b, Step 2), the resulting $\mathbf{P_{STATION}}^{*-}$:**3-NDI-ring** species transfers an electron to the **3-NDI-ring** within the pseudorotaxane (Fig. 1b, Step 3), yielding $\mathbf{P_{STATION}}$:**3-NDI-ring**$^{\bullet-}$. Upon reduction the **3-NDI-ring**$^{\bullet-}$ loses its affinity for the thread of $\mathbf{P_{STATION}}$ and is replaced by a neutral **3-NDI-ring** from the bulk electrolyte. The reduced **3-NDI-ring**$^{\bullet-}$ is thus actively repelled from the NiO–dye interface (launching effect (2), Fig. 1b, Step 4), preventing charge recombination (Fig. 1c, Pathway 5). The launched **3-NDI-ring**$^{\bullet-}$ is regenerated at counter electrode leading to photocurrent (Fig. 1b, Step 5–6). It is therefore anticipated that the creation of unidirectional charge propagation at a molecular level should translate to macroscopic charge rectification in the device, which should inhibit both recombination pathways (Fig. 1c, Pathway 5–6) resulting in enhanced V_{OC}, J_{SC} and therefore improve PCE.

The **P1** dye[29] and the $\mathbf{P_{STATION}}$ dye[14] were synthesized according to literature. The absorption maximum of the $\mathbf{P_{STATION}}$ (λ_{max} = 455 nm) experiences a blue shift compared to **P1** (λ_{max} = 472 nm) (Fig. 2a). This particular absorption, derived from an intramolecular charge transfer (ICT) in the dyes highlights the decrease in respective acceptor strength (i.e., cyanoacrylate in $\mathbf{P_{STATION}}$ vs (dicyano)vinyl in **P1**) between molecules. The **3-NDI-ring** was synthesized in two steps, employing Mitsunobu coupling to effect ring closure between pyromellitic diimide and the **3-NDI** fragment in 31% isolated yield (Supplementary Sect. 1.2).

Binding of **3-NDI-ring** to the **DNP** recognition site within $\mathbf{P_{STATION}}$ were prohibited by limited solubility of the dye, therefore the recognition site moiety **DNP-thread** (Fig. 2d) was used to analyze pseudorotaxane formation by ^{1}H NMR titration. A typical upfield shift (0.5 ppm) in the ^{1}H NMR spectra for the aromatic protons of the **3-NDI-ring** in CD_2Cl_2 was observed (Supplementary Fig. 6).[27] Fitting the titration curve to a model for 1:1 binding revealed an association constant (K_a) of 210 M^{-1}. Pseudorotaxane formation between the electron rich and deficient components typically leads to charge transfer (CT) band at visible wavelengths. UV–Vis spectrophotometry in a valeronitrile/MeCN (15:85) solution of **DNP-thread**:**3-NDI-ring** (10:1) indeed revealed the characteristic CT band evolving at 460 nm in line with pseudorotaxane formation (Fig. 2b).[30] The K_a ascertained from ^{1}H NMR was complemented by spectrophotometry by

probing the formation of the **DNP-thread:3-NDI-ring** complex by UV–Vis titration (Fig. 2d). The spectral overlap of the $P_{STATION}$ ICT absorption (λ = 455 nm) precluded observation of the CT evolving from pseudorotaxane formation (λ = 460 nm) over the course of the titration.

Monitoring the absorption at λ = 460 nm UV–vis at 460 nm and fitting to a 1:1 binding model afforded a K_a = 160 M^{-1} for the **DNP-thread**:**3-NDI-ring** pseudorotaxane (Fig. 2c, Table 1). The differences between K_a derived from NMR and UV–Vis were rationalized by the difference in solvent polarity (CD_2Cl_2 vs. valeronitrile/MeCN (15:85) respectively). Immobilization of $P_{STATION}$ onto NiO electrodes (*vide infra*, Supplementary Fig. 13) and immersion into a **3-NDI-ring** solution (20 μM in MeCN) led to a decrease in **3-NDI-ring** absorption intensity at λ = 378 nm. Given that the control experiment with **P1** in place of $P_{STATION}$ (Supplementary Fig. 14) experienced no absorption drop at 378 nm, we could ascribe the absorption decreases to the binding of **3-NDI-ring** to the **DNP** recognition sites of the $P_{STATION}$-NiO.

Cyclic voltammetry (CV, Supplementary Fig. 8) of **3-NDI-ring** revealed four reductions, attributed to two independent reduction events at the NDI and two at the pyromellitic moieties of the **3-NDI-ring**. The redox events were fully reversible, demonstrating electrochemical stability, which is an important requirement for redox mediators in DSSCs. The first reduction potential of the **3-NDI-ring** (-0.35 V vs. NHE) is 0.55 V lower than that of $P_{STATION}^{*-}$ (Fig. 1d), facilitating exergonic electron transfer from $P_{STATION}^{*-}$ to **3-NDI-ring**. CV of the **DNP-thread**:**3-NDI-ring** complex shows that binding of the **DNP-thread** to the **3-NDI-ring** has a small effect on the reduction potential (40 mV). Importantly, scan rate dependent CV experiments demonstrate that reduction of **3-NDI-ring** in the model **DNP-thread**:**3-NDI-ring** prompts a loss of affinity and unbinding from the **DNP-thread** (Supplementary Fig. 9).[31] This “ring launching” effect reflected by the 40 mV reduction potential decrease, is only observed for the first reduction event of the **3-NDI-ring** when bound to the **DNP-thread** (-0.39 V vs. NHE compared to -0.35 V vs. NHE for the free **3-NDI-ring** (Supplementary Table 2). The absence of this typical shift in the three subsequent reduction events show that the mono-reduced ring **3-NDI-ring**$^{\bullet-}$ unbinds **DNP-thread** after the first reduction.

Table 1
Summary of the optical and electrochemical properties of **P1** and $P_{STATION}$ (0.5 mM) in MeCN.[14] The redox potentials (vs. NHE) are determined in 0.1 M $TBAPF_6$ with a glassy carbon working electrode, a leakless Ag/AgCl reference electrode and a Pt wire counter electrode.

Molecule	λ_{max} (nm)	ε (× 10^4 M^{-1} cm^{-1})	E_{0-0} (eV)	$E_{D^*/D}$	E_{D/D^-}	ΔG°
P1	472	5.8	2.27	1.30	-0.77	-0.42
$P_{STATION}$	455	6.4	3.30	1.32	-0.98	-0.63

Photovoltaic performance. To explore if the pseudorotaxane strategy leads to increased photovoltaic performance, *p*-DSSCs were prepared using NiO photocathodes (3.5 μm, active area 0.196 cm^{-2})

functionalized with **P1** or $\mathbf{P_{STATION}}$ by sensitizing in MeCN solution for 16 hours. Measurement of dye loading by uptake experiments revealed that the surface coverage of **P1** (Γ=7.03× 10^{-8} mol cm^{-2}) is approximately 50% higher than that of $\mathbf{P_{STATION}}$ (Γ= $\mathbf{P_{STATION}}$ 4.50 × 10^{-8} mol cm^{-2}), rationalized by the larger molecular size of $\mathbf{P_{STATION}}$ as it is equipped with the **DNP** recognition site (r_H = 0.68 nm for $\mathbf{P_{STATION}}$ versus r_H = 0.39 nm for **P1**, Supplementary Table 1). The devices were assembled with poly(3,4-ethylenedioxythiophene) (PEDOT) counter electrodes using a 60 µm thermoplast frame (Meltonix polymer 1170-60) and loaded with the **3-NDI-ring** electrolyte (25 mM **3-NDI-ring/3-NDI-ring**$^{\bullet-}$, 1:1 in 1 M LiTFSI valeronitrile/MeCN (15:85)) inside a nitrogen filled glovebox. The photovoltaic performances of DSSCs based on $\mathbf{P_{STATION}}$ and **P1** were evaluated under AM1.5G illumination (100 mW cm^{-2}) and are represented in Fig. 3 and summarized in Table 2. The DSSCs based on the pseudorotaxane strategy, the $\mathbf{P_{STATION}}$:**3-NDI-ring** system outperforms the **P1** reference system, in all photovoltaic parameters, with 123 mV enhancement in open circuit voltage (V_{OC}) (208 mV in **P1** vs. 331 mV in $\mathbf{P_{STATION}}$) and a tripling of short circuit current density (J_{SC}) (0.143 mA cm^2 in **P1** vs. 0.388 mA cm^2 in $\mathbf{P_{STATION}}$,), leading to a fivefold increase in PCE (0.009% in **P1** vs. 0.048% in $\mathbf{P_{STATION}}$). The photocurrent action spectrum of $\mathbf{P_{STATION}}$ reveals a higher incident photon-to-current conversion efficiency (IPCE) across the spectrum (Fig. 3b) with a maximum of 5.3% at 475 nm versus the **P1** system ($IPCE_{max}$ = 2.6% at 500 nm). The improved fill factor (FF) in the $\mathbf{P_{STATION}}$:**3-NDI-ring** based cells compared to the **P1** reference system in combination with the higher V_{OC}, suggests reduced charge recombination as a result of preorganization of the redox mediator to the dye via pseudorotaxane formation.

Table 2
Summary of the photovoltaic performance data for DSSC based on **P1** and $\mathbf{P_{STATION}}$ under AM 1.5G illumination (100 mW cm^{-2}) with the **3-NDI-ring** electrolyte (25 mM) in 1 M LiTFSI valeronitrile/MeCN (15:85). The average performance (N = 9 for **P1** and $\mathbf{P_{STATION}}$) is provided with the best performing cell in brackets.

Dye	V_{OC} (mV)	J_{SC} (mA cm^{-2})	FF	PCE (%)
P1	208 ± 23 (210)	0.143 ± 0.044 (0.146)	0.311 ± 0.050 (0.361)	0.009 ± 0.006 (0.015)
$\mathbf{P_{STATION}}$	331 ± 53 (385)	0.388 ± 0.112 (0.500)	0.359 ± 0.057 (0.412)	0.048 ± 0.013 (0.060)

Chopped light amperometry experiments were performed, where the light is switched on and off in periods of 10 seconds with an increasing illumination density starting from 5 mW cm^{-2} to 50 mW cm^{-2} at short current conditions. For both solar cells the J_{SC} increases with the light intensity, as expected for these DSSCs (Fig. 3c), and the larger increase of the $\mathbf{P_{STATION}}$:**3-NDI-ring** based cell is in line with the better performance. Interestingly, the shape of the photocurrent response for the **P1** shows tailing behavior that

increases with light intensity. This indicates mass transfer limitations of the redox mediator through the mesoporous electrode (Fig. 3c inset), which can be expected for large molecules like **3-NDI-ring** at low concentrations.[32,33] This tailing behavior is not observed for $\mathbf{P_{STATION}}$ based DSSCs in line with preorganization of the redox mediator and efficient replacement of reduced **3-NDI-ring**$^{\bullet-}$ for neutral **3-NDI-ring**^{0}, leading to high local concentrations of **3-NDI-ring** at the dye–electrolyte interface even at very low (25 mM) concentrations of redox mediator.

Differences in solar cell performance originating from pseudorotaxane formation were further probed by electrochemical impedance spectroscopy (EIS). Performing EIS under varying light intensities affords insight into electron–hole recombination at the semiconductor–dye interface through determination of the hole lifetime (τ_h) as a function of V_{OC} (Fig. 3d).[34] At any given V_{OC} the hole lifetime for $\mathbf{P_{STATION}}$ (624 ms at 0.1 V) is two times longer than **P1** (324 ms at 0.1 V), implying that less recombination occurs in the pseudorotaxane system. This could either arise from a difference in recombination resistance (R_{REC}) or from a change in chemical capacitance (C_μ), originating from a valence band shift.[35] The C_μ (Supplementary Fig. 25) shows no dependency on the applied voltage and a minimal shift between the **P1** and $\mathbf{P_{STATION}}$ DSSCs, expected given the similarity of the systems, thus cannot be the reason for V_{OC} enhancements in $\mathbf{P_{STATION}}$:**3-NDI-ring** *p*-DSSCs. The measured R_{REC} for the $\mathbf{P_{STATION}}$ system (3.20×10^5 Ω cm^{-2} at 0.1 V) is higher than for **P1** (2.93×10^5 Ω cm^{-2} at 0.1 V) meaning that the difference in hole lifetime originates from lower recombination at the semiconductor–electrolyte interface. This effect further supports the active charge rectification bestowed $\mathbf{P_{STATION}}$:**3-NDI-ring** *p*-DSSCs by introducing molecular machinery to the influence the preorganization and replacement of the redox mediator in the solar cell.

Conclusion

Charge recombination is one of the key issues to solve in the area of *p*-DSSCs, and inspired by binding/unbinding events of redox mediators in natural photosynthesis, we studied if molecular machinery can be implemented in *p*-DSSC to facilitate directional electron transport to reduce charge recombination. The $\mathbf{P_{STATION}}$ dye based on the **P1** benchmark system is equipped with a docking station for preorganization of ring-shaped redox mediator (**3-NDI-ring)** that form pseudorotaxanes. Reduction of **3-NDI-ring** by electron transfer in $\mathbf{P_{STATION}}^{*-}$:**3-NDI-ring** pseudorotaxane prompts disassembly of the supramolecular complex resulting in ring launching of the reduced mediator, making space for a new neutral redox mediator to bind. The *p*-DSSCs based on $\mathbf{P_{STATION}}$:**3-NDI-ring** pseudorotaxanes exhibit enhanced performance across all photovoltaic parameters in comparison to the **P1**, which does not facilitate preorganization of the **3-NDI-ring** mediator. Chopped light amperometry and EIS under varying light intensities showed that both preorganization and ring launching contributes to lowering recombination and a twofold extension to hole lifetimes, leading to a higher V_{OC} and 5 times increase in PCE in *p*-DSSC. We envision that this bio-inspired approach to integrate artificial molecular machinery in

p-DSSCs for supramolecular charge-transfer rectification is a strategy that could be expanded to other PEC devices for solar energy conversion technologies.

Declarations

Acknowledgements

This study was supported by the Holland Research School for Molecular Sciences (HRSMC) and the University of Amsterdam. We would like to thank AMOLF for SEM imaging and Wojciech Sikorski for BET analysis of the NiO.

Author Contributions

T.B. and J.R. proposed the research. T.B. synthesized and characterized the dyes, the macrocycle and pseudorotaxane assisted by J.H. and M.D. DSSC fabrication and characterization was performed by T.B. EIS measurements were performed by T.B. and analyzed by T.M.B. Experiments were designed by T.B., S.M., T.M.B. and J.R. The manuscript was prepared by T.B. S.M. and J.R. with assistance of T.M.B.

Competing Interests statement

The authors declare no competing interests.

References

1. Dau, H. & Zaharieva, I. Principles, efficiency, and blueprint character of solar-energy conversion in photosynthetic water oxidation. *Acc. Chem. Res.* **42**, 1861–1870 (2009).
2. Zhang, B. & Sun, L. Artificial photosynthesis: opportunities and challenges of molecular catalysts. *Chem. Soc. Rev.* **48**, 2216–2264 (2019).
3. Croce, R. & van Amerongen, H. Natural strategies for photosynthetic light harvesting. *Nat. Chem. Biol.* **10**, 492–501 (2014).
4. Van Eerden, F. J., Melo, M. N., Frederix, P. W. J. M., Periole, X. & Marrink, S. J. Exchange pathways of plastoquinone and plastoquinol in the photosystem II complex. *Nat. Commun.* **8**, 1–8 (2017).
5. Kulik, N., Kutý, M. & Řeha, D. The study of conformational changes in photosystem II during a charge separation. *J. Mol. Model.* **26**, 75 (2020).
6. Kakiage, K. *et al.* Highly-efficient dye-sensitized solar cells with collaborative sensitization by silyl-anchor and carboxy-anchor dyes. *Chem. Commun.* **51**, 15894–15897 (2015).
7. Mori, S. *et al.* Charge-transfer processes in dye-sensitized NiO solar cells. *J. Phys. Chem. C* **112**, 16134–16139 (2008).
8. Nakade, S. *et al.* Influence of TiO 2 Nanoparticle Size on Electron Diffusion and Recombination in Dye-Sensitized TiO 2 Solar Cells. *J. Phys. Chem. B* **107**, 8607–8611 (2003).

9. Morandeira, A., Boschloo, G., Hagfeldt, A. & Hammarström, L. Photoinduced ultrafast dynamics of coumarin 343 sensitized p-type-nanostructured NiO films. *J. Phys. Chem. B* **109**, 19403–19410 (2005).
10. Daeneke, T. *et al.* Dominating Energy Losses in NiO p-Type Dye-Sensitized Solar Cells. *Adv. Energy Mater.* **5**, 1401387 (2015).
11. Parlane, F. G. L. *et al.* Spectroscopic detection of halogen bonding resolves dye regeneration in the dye-sensitized solar cell. *Nat. Commun.* **8**, 1761 (2017).
12. Uemura, Y., Murakami, T. N. & Koumura, N. Crown Ether-Substituted Carbazole Dye for Dye-Sensitized Solar Cells: Controlling the Local Ion Concentration at the TiO 2 /Dye/Electrolyte Interface. *J. Phys. Chem. C* **118**, 16749–16759 (2014).
13. Wood, C. J. *et al.* Red-Absorbing Cationic Acceptor Dyes for Photocathodes in Tandem Solar Cells. *J. Phys. Chem. C* **118**, 16536–16546 (2014).
14. Bouwens, T., Mathew, S. & Reek, J. N. H. p-Type dye-sensitized solar cells based on pseudorotaxane mediated charge-transfer. *Faraday Discuss.* **215**, 393–406 (2019).
15. Cheng, C. *et al.* An artificial molecular pump. *Nat. Nanotechnol.* **10**, 547–553 (2015).
16. Cai, K. *et al.* Molecular-Pump-Enabled Synthesis of a Daisy Chain Polymer. *J. Am. Chem. Soc.* **142**, 10308–10313 (2020).
17. Simpson, C. D. *et al.* Nanosized Molecular Propellers by Cyclodehydrogenation of Polyphenylene Dendrimers. *J. Am. Chem. Soc.* **126**, 3139–3147 (2004).
18. Fennimore, A. M. *et al.* Rotational actuators based on carbon nanotubes. *Nature* **424**, 408–410 (2003).
19. Kassem, S., Lee, A. T. L., Leigh, D. A., Markevicius, A. & Solà, J. Pick-up, transport and release of a molecular cargo using a small-molecule robotic arm. *Nat. Chem.* **8**, 138–143 (2016).
20. Jiménez, M. C., Dietrich-Buchecker, C. & Sauvage, J. Towards Synthetic Molecular Muscles: Contraction and Stretching of a Linear Rotaxane Dimer. *Angew. Chemie* **39**, 3284–3287 (2000).
21. Juluri, B. K. *et al.* A mechanical actuator driven electrochemically by artificial molecular muscles. *ACS Nano* **3**, 291–300 (2009).
22. Kudernac, T. *et al.* Electrically driven directional motion of a four-wheeled molecule on a metal surface. *Nature* **479**, 208–211 (2011).
23. Lehn, J. M. From supramolecular chemistry towards constitutional dynamic chemistry and adaptive chemistry. *Chem. Soc. Rev.* **36**, 151–160 (2007).
24. Lehn, J. M. Perspectives in chemistry - Steps towards complex matter. *Angew. Chemie Int. Ed.* **52**, 2836–2850 (2013).
25. Ashton, P. R. *et al.* A light-fueled 'piston cylinder' molecular-level machine [5]. *J. Am. Chem. Soc.* **120**, 11190–11191 (1998).
26. Saha, S. *et al.* A Photoactive Molecular Triad as a Nanoscale Power Supply for a Supramolecular Machine. *Chem. Eur. J.* **11**, 6846–6858 (2005).

27. Scott Lokey, R. & Iverson, B. L. Synthetic molecules that fold into a pleated secondary structure in solution. *Nature* **375**, 303–305 (1995).
28. Wilson, H., Byrne, S. & Mullen, K. M. Dynamic Covalent Synthesis of Donor-Acceptor Interlocked Architectures in Solution and at the Solution:Surface Interface. *Chem. Asian J.* **10**, 715–721 (2015).
29. Qin, P. *et al.* Design of an Organic Chromophore for P-Type Dye-Sensitized Solar Cells (vol 130, pg 8570, 2008). *J. Am. Chem. Soc.* **130**, 17629 (2008).
30. Olsen, J. C. *et al.* A neutral redox-switchable [2]rotaxane. *Org. Biomol. Chem.* **9**, 7126–7133 (2011).
31. Fahrenbach, A. C. *et al.* Measurement of the ground-state distributions in bistable mechanically interlocked molecules using slow scan rate cyclic voltammetry. *Proc. Natl. Acad. Sci.* **108**, 20416–20421 (2011).
32. Nelson, J. J., Amick, T. J. & Elliott, C. M. Mass transport of polypyridyl cobalt complexes in dye-sensitized solar cells with mesoporous TiO2 photoanodes. *J. Phys. Chem. C* **112**, 18255–18263 (2008).
33. Yella, A. *et al.* Dye-sensitized solar cells using cobalt electrolytes: the influence of porosity and pore size to achieve high-efficiency. *J. Mater. Chem. C* **5**, 2833–2843 (2017).
34. Huang, Z., Natu, G., Ji, Z., Hasin, P. & Wu, Y. p-Type Dye-Sensitized NiO Solar Cells: A Study by Electrochemical Impedance Spectroscopy. *J. Phys. Chem. C* **115**, 25109–25114 (2011).
35. Fabregat-Santiago, F., Bisquert, J., Palomares, E., Haque, S. A. & Durrant, J. R. Impedance spectroscopy study of dye-sensitized solar cells with undoped spiro-OMeTAD as hole conductor. *J. Appl. Phys.* **100**, 034510 (2006).

Figures

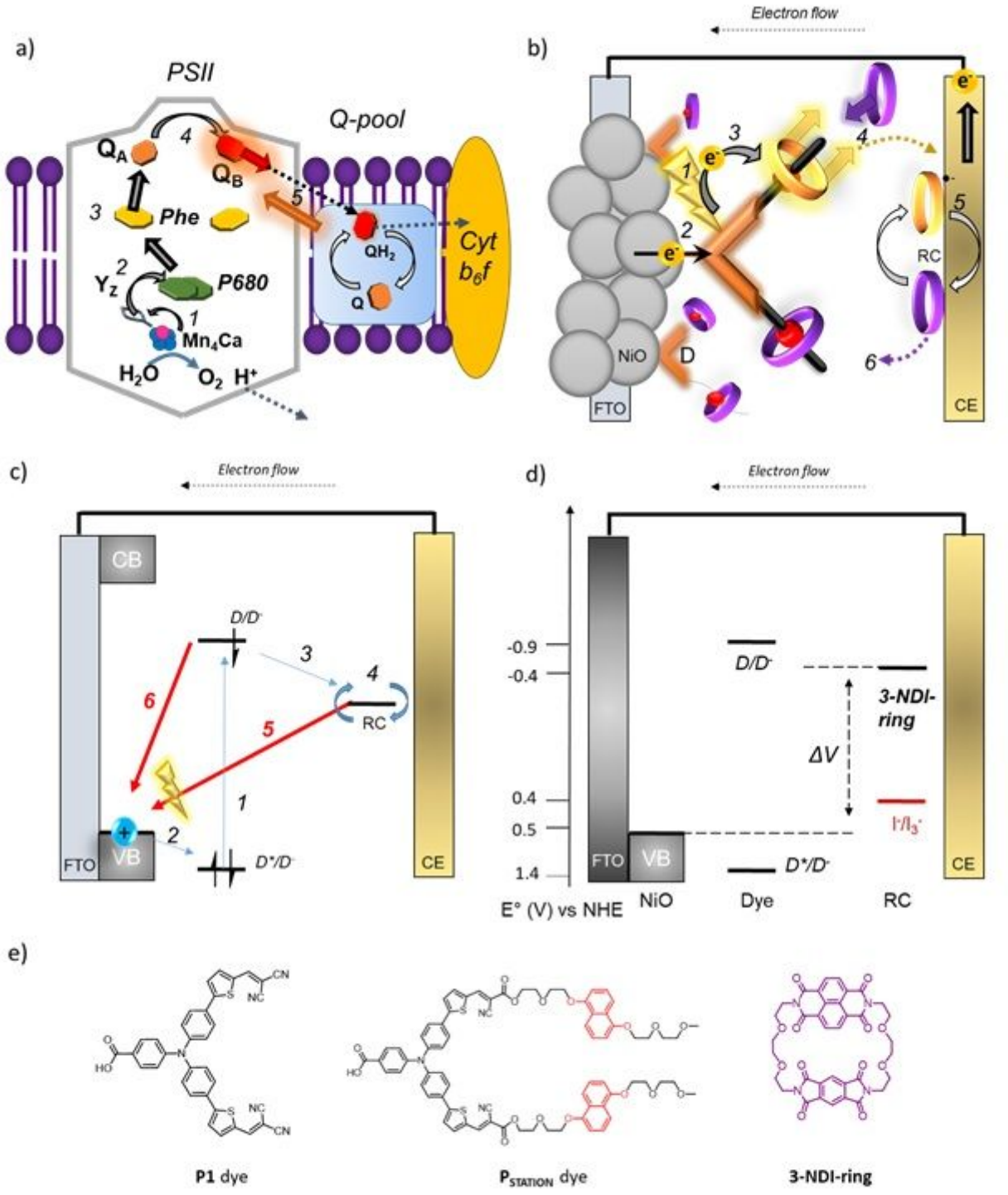

Figure 1

Similarities between the electron propagation in PSII and the pseudorotaxane based DSSC. a) Electrons are extracted from water (1) after photoexcitation of the pigment P680 and pheophytin (Phe) (2) leading to electron transfer to QA and terminal quinone QB (4). Conversion of QB to hydroquinone leads to its replacement by a new quinone (5). The hydroquinone is regenerated by the cytochrome b6f complex. b) Schematic representation of the pseudorotaxane based DSSC. The pigment in this artificial system is the

PSTATION dye with docking stations for the redox mediator, the macrocycle (3-NDI-ring). Upon photoexcitation of the dye (1) and hole injection into NiO (2), the electron is transferred reducing 3-NDI-ring (3), which is subsequently replaced by a neutral ring (purple), effectively removing the charged ring from the NiO–dye interface, thereby preventing charge recombination. (4) The regeneration of the electron acceptor occurs at the counter electrode of the device (5,6). c) Schematic representation of the forward electron propagation (1–4) and the recombination pathways 5 and 6. d) Schematic energy diagram for the p-DSSC based on the PSTATION pseudorotaxane dye. Energy levels are represented in V (vs. NHE). FTO = fluorine doped tin oxide; VB = valence band; CB = conduction band; D = dye; RC = redox couple; CE= counter electrode. e) Chemical structures of molecular dyes P1 and PSTATION, the latter featuring binding sites to facilitate pseudorotaxane formation with the macrocycle 3-NDI-ring.

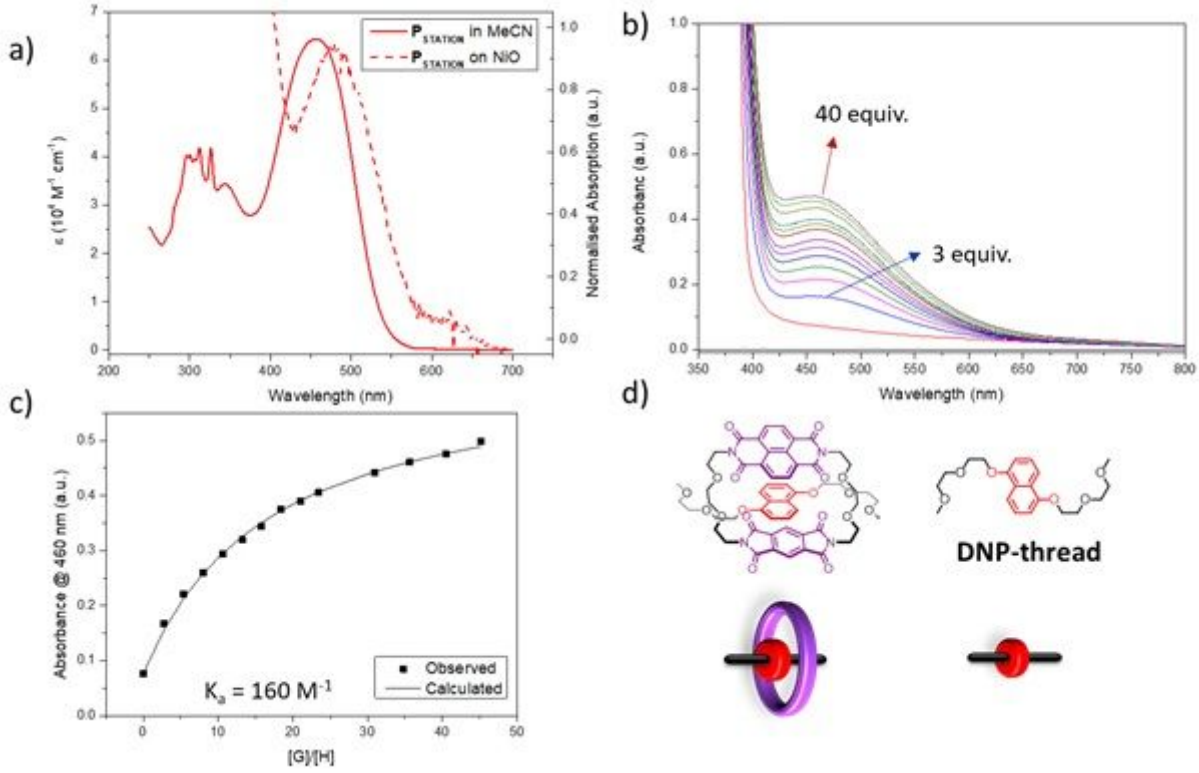

Figure 2

a) UV–Vis spectra of PSTATION in solution (solid line) and adsorbed onto NiO (dashed line). b) Emergence of CT band upon addition of DNP recognition site to 3-NDI-ring (49.5 μM) indicating pseudorotaxane formation in valeronitrile/MeCN (15:85). c) The titration curve was used to determine the Ka. d) Structure of the DNP-thread and the DNP-thread:3-NDI-ring pseudorotaxane.

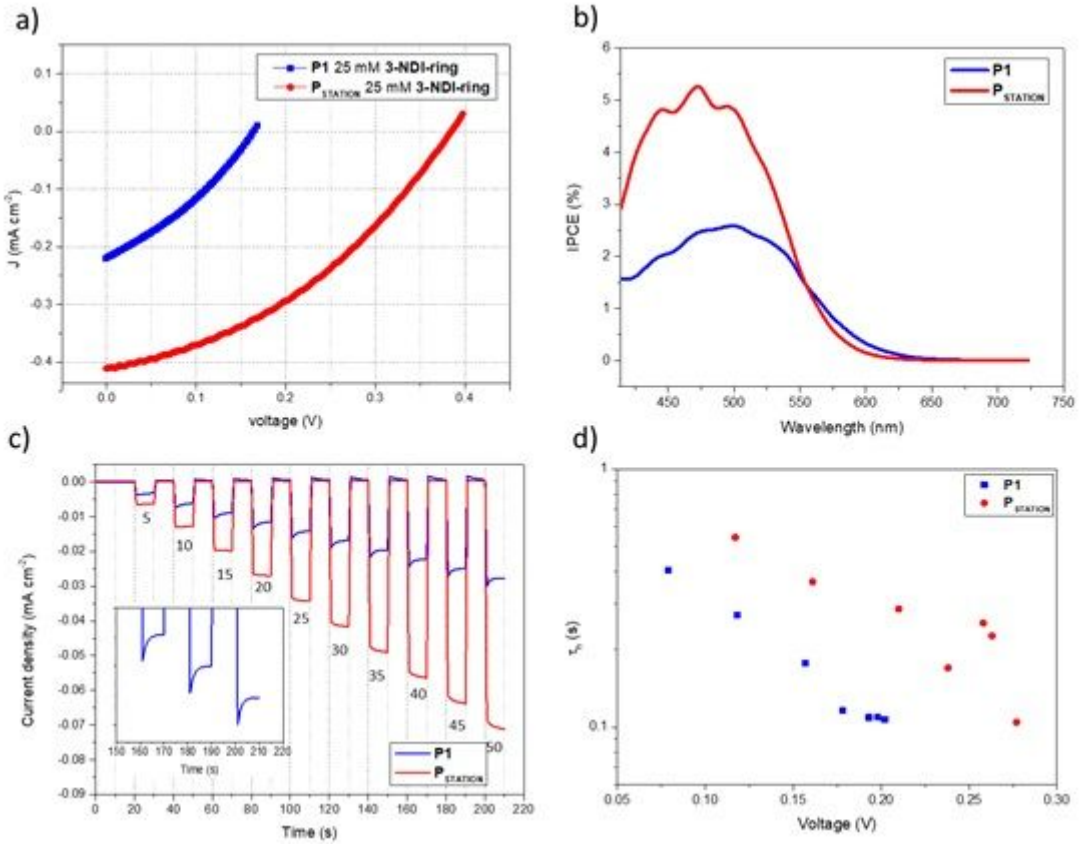

Figure 3

a) Photovoltaic performances of the devices based on the P1 (blue squares) and the PSTATION dye (red dots) with the 3-NDI-ring as redox mediator (25 mM in 1 M LiTFSI) which can only form pseudorotaxanes with the PSTATION dye. b) A photocurrent action spectrum of the PSTATION based system (red) and the P1 based system (blue). c) Chopped light amperometry at different light flux varying from 5–50 mW cm-2 with on/off cycles of 10 seconds. The insert graph displays the decay effect (tailing behavior) observed in the P1 based system for the photocurrent at 40, 45 and 50 mW cm-2. d) Hole lifetime τh as function of VOC obtained through EIS measurements under varying light intensities measured on the P1 system (blue) and the PSTATION system (red).

Supplementary Files

This is a list of supplementary files associated with this preprint. Click to download.

- ReeketaI3NDIringDSSCSUppinfo.pdf